Available online at http://scik.org
Commun. Math. Biol. Neurosci. 2025, 2025:129
https://doi.org/10.28919/cmbn/9495
ISSN: 2052-2541

DYNAMICAL ANALYSIS AND OPTIMAL CONTROL OF A MALARIA TRANSMISSION MODEL WITH VACCINATION

JONNER NAINGGOLAN[1,*], MOCH. FANDI ANSORI[2], HASMI[3]

[1]Department of Mathematics, Faculty of Mathematics and Natural Sciences, Universitas Cenderawasih, Jayapura, 99224, Indonesia

[2]Department of Mathematics, Faculty of Science and Mathematics, Universitas Diponegoro, Semarang, 50275, Indonesia

[3]Department of Public Health, Faculty of Public Health, Universitas Cenderawasih, Jayapura, 99224, Indonesia

Abstract. This study develops and analyzes a compartmental model for optimizing malaria control strategies, with particular emphasis on the role of vaccination. The model captures key epidemiological dynamics, including resusceptibility, drug resistance, and vaccination, and incorporates three time-dependent control interventions: preventive measures, vaccination enhancement, and treatment efforts. The basic reproduction number is analytically derived to characterize the threshold conditions for disease persistence. Local and global stability analyses of the nonendemic equilibrium are carried out, providing theoretical assurance that the disease can be eradicated when the reproduction number is below unity. Parameter values are obtained from regional data and literature sources. A local sensitivity analysis based on elasticity indices identifies the most influential parameters affecting the basic reproduction number, notably the transmission rates between humans and mosquitoes and the treatment rate for drug-sensitive infections. Contour plots further illustrate the joint effects of key parameters on disease transmission potential. Optimal control strategies are derived using Pontryagin's Maximum Principle and validated through numerical simulations. The results demonstrate that vaccination significantly reduces the number of

*Corresponding author
E-mail address: jonner2766@gmail.com
Received July 15, 2025

infected individuals and enhances overall disease suppression, particularly when implemented alongside prevention and treatment controls. These findings underscore the importance of integrating vaccination with other public health interventions to design effective and cost-efficient malaria control programs.

Keywords: malaria transmission model; vaccination; optimal control; sensitivity analysis.

2020 AMS Subject Classification: 92D30, 49K15, 34D20.

1. INTRODUCTION

Malaria, caused by parasites of the genus *Plasmodium* and transmitted through the bites of infected *Anopheles* mosquitoes, remains one of the most persistent global public health threats. According to the World Health Organization (WHO), over 249 million malaria cases were reported in 2022—five million more than in 2021—surpassing the pre-COVID-19 estimates [1]. This resurgence underscores the need for more effective and targeted interventions, particularly in endemic regions.

Mathematical modeling has become an essential tool for understanding the dynamics of malaria transmission and formulating strategies for its control. Such models facilitate the prediction of outbreak patterns, identification of key transmission parameters [2, 3], sensitivity analysis [4], qualitative behavior of solutions including the potential for disease eradication or persistence [5], and control strategies [6]. Discrete and continuous-time models have been applied to capture complex biological and environmental interactions that drive malaria epidemiology.

In regions such as Papua Province, Indonesia, malaria control is further challenged by the presence of drug-resistant *Plasmodium* strains [7]. Previous studies have incorporated features such as mosquito reinfection [8, 9], drug resistance [10, 11], and combined interventions including treatment and vector control [12].

This study employed a compartmental modeling framework grounded in SEIR-type dynamics [13], wherein both human and mosquito populations are stratified into epidemiologically relevant subgroups. Prior research has explored various extensions of this framework, including SIR-type models that incorporate multiple parasite strains in the human host and corresponding SI models for mosquito vectors [14, 15]. SEIR-based models have also been used to analyze the effectiveness of vaccination and optimal treatment strategies [16]. Other contributions include

the use of SEIR models for human populations coupled with SEI dynamics for mosquitoes [17] and the introduction of SWEIR-type models, where the additional compartment W represents individuals with heightened awareness of malaria infection [18]. Moreover, several studies investigated optimal intervention strategies that encompass both treatment and resistance-driven control measures [19, 20].

Of particular relevance is the recent deployment and testing of pre-erythrocytic malaria vaccines in Papua and West Papua, Indonesia. Using local epidemiological data, studies have applied nonlinear least-squares estimation to calibrate model parameters [21, 22], highlighting the inadequacy of existing interventions and the need for strengthened measures, such as bed net usage, environmental control, and community engagement [23].

Building on prior work [24], this study introduced a vaccinated subpopulation into a malaria transmission model and evaluated the effectiveness of multiple control strategies. These include preventive measures (e.g., mosquito screens and bed nets), enhancement of vaccination impact through nutritional support (e.g., vitamin supplementation), and optimized treatment aimed at shortening the recovery duration. The model was specifically tailored to the epidemiological context of Papua Province, where recent vaccination trials are supported by national health authorities. Through mathematical analysis and numerical simulation, we aimed to identify optimal control strategies that minimize infection and enhance recovery while considering both biological dynamics and practical intervention constraints.

2. Mathematical Model of Malaria Spread

The model developed in this study builds on a previous SEIR-type compartmental framework and divides the population into nine subpopulations. The human population was classified into seven epidemiologically distinct groups. These include $S(t)$, representing susceptible individuals who are healthy and vulnerable to malaria infection; $V(t)$, denoting vaccinated individuals who have received the malaria vaccine; $I_s(t)$, comprising malaria-infected individuals who are sensitive to antimalarial drugs; $I_r(t)$, representing infected individuals who are resistant to antimalarial drugs; $I_{st}(t)$, referring to drug-sensitive infected individuals who have undergone treatment; $I_{rt}(t)$, representing drug-resistant infected individuals who have received treatment; and $R(t)$, which denotes recovered individuals who have acquired immunity to malaria. The

mosquito population is divided into two groups: $X(t)$, which represents susceptible mosquitoes that have not yet been infected by the *Plasmodium* parasite, and $Y(t)$, which represents infected mosquitoes that carry the *Plasmodium* parasite and are capable of transmitting the disease.

The model is based on the following assumptions. First, the total population was assumed to remain constant over time. Second, vaccinated individuals who do not come into contact with infected mosquitoes are considered to have gained immunity, whereas those who may still become infected. Third, malarial infections are transmitted through contact between mosquitoes and either susceptible or vaccinated humans. Fourth, individuals who become infected are assumed to eventually recover and transition to the recovered class following treatment. Susceptible mosquitoes become infected when they bite an infected human host.

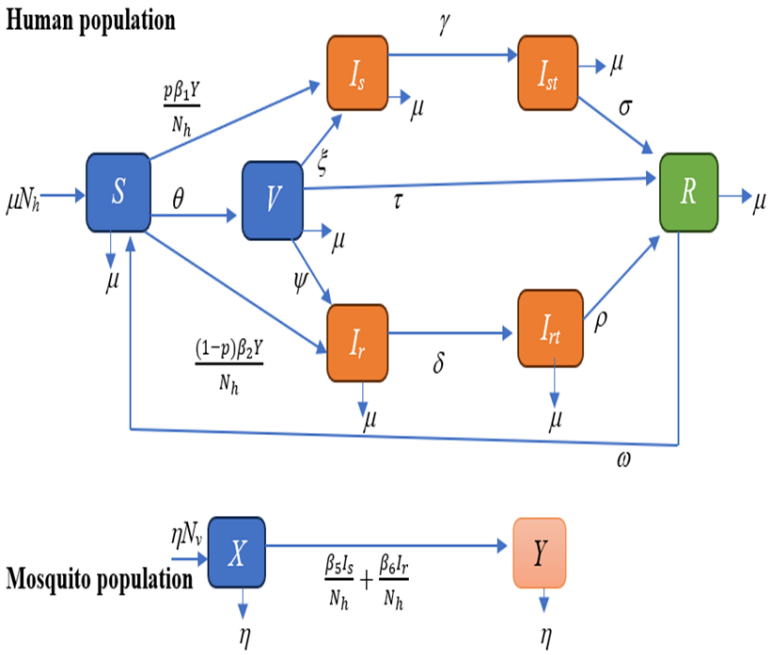

FIGURE 1. A schematic diagram illustrating the spread of malaria with vaccination factors.

Based on these assumptions, a schematic diagram of the disease transmission is shown in Fig. 1. Based on this figure, we have the following system of differential equations describing the dynamics of malaria transmission:

$$\frac{dS}{dt} = \mu N_h - \left(\theta + \frac{p\beta_1}{N_h}Y + \frac{(1-p)\beta_2}{N_h}Y + \mu\right)S + \omega R, \tag{1a}$$

$$\frac{dV}{dt} = \theta S - \left(\frac{q\beta_3}{N_h}Y + \frac{(1-q)\beta_4}{N_h}Y + \tau + \mu\right)V, \tag{1b}$$

$$\frac{dI_s}{dt} = \frac{p\beta_1}{N_h}SY + \frac{q\beta_3}{N_h}VY - (\gamma+\mu)I_s, \tag{1c}$$

$$\frac{dI_r}{dt} = \frac{(1-p)\beta_2}{N_h}SY + \frac{(1-q)\beta_4}{N_h}VY - (\delta+\mu)I_r, \tag{1d}$$

$$\frac{dI_{st}}{dt} = \gamma I_s - (\sigma+\mu)I_{st}, \tag{1e}$$

$$\frac{dI_{rt}}{dt} = \delta I_r - (\rho+\mu)I_{rt}, \tag{1f}$$

$$\frac{dR}{dt} = \tau V + \sigma I_{st} + \rho I_{rt} - (\omega+\mu)R, \tag{1g}$$

$$\frac{dX}{dt} = \eta N_v - \left(\frac{\beta_5}{N_h}I_s + \frac{\beta_6}{N_h}I_r + \eta\right)X, \tag{1h}$$

$$\frac{dY}{dt} = \left(\frac{\beta_5}{N_h}I_s + \frac{\beta_6}{N_h}I_r\right)X - \eta Y, \tag{1i}$$

where

$$N_h = S + V + I_s + I_r + I_{st} + I_{rt} + R \text{ and } N_v = X + Y.$$

Model (1) has a nonnegative initial condition as follows:

$$S(0) > 0, V(0) \geq 0, I_s(0) \geq 0, I_r(0) \geq 0, I_{st}(0) \geq 0, I_{rt}(0) \geq 0, R(0) \geq 0,$$

$$X(0) > 0, Y(0) \geq 0.$$

The parameters used in the model (1) are defined in Table 1.

TABLE 1. Parameter descriptions and values for the malaria transmission model.

Symbol	Description	Value	Reference
μ	Natural birth/death rate	4.19175×10^{-5}	[22]
ω	Resusceptibility rate	0.025	[6]
θ	Vaccination rate	0.001	[21]
p	Proportion exposed to sensitive strain	0.59999	[21]
q	Proportion of vaccinated exposed to sensitive strain	0.29999	[21]
β_1	Transmission rate (sensitive) for S	0.4	assumed
β_2	Transmission rate (resistant) for S	0.4	assumed
β_3	Transmission rate (sensitive) for V	2.37749×10^{-6}	[21]
β_4	Transmission rate (resistant) for V	1.11742×10^{-6}	[21]
τ	Recovery rate of vaccinated	0.53	[21]
γ	Treatment rate for sensitive infected	0.049999	assumed
δ	Treatment rate for resistant infected	0.05	assumed
σ	Recovery rate for treated sensitive infected	5×10^{-9}	[10]
ρ	Recovery rate for treated resistant infected	5×10^{-9}	[10]
η	Birth/death rate of mosquitoes	variable	[6]
β_5	Infection rate of mosquitoes (sensitive)	0.48	[6]
β_6	Infection rate of mosquitoes (resistant)	0.24	assumed

To ensure the epidemiological feasibility of the malaria model (1), it is essential to demonstrate that solutions remain within biologically meaningful bounds over time. The theorem below outlines the positive criteria for the solution of model (1). The proof is presented in accordance with the style in [25].

Theorem 1. *Assume that all model parameters in system* (1) *are nonnegative and that the initial conditions are both nonnegative and finite. Then, every solution of model* (1) *remains nonnegative for any* $t > 0$.

Proof. According to model (1), at the boundary of set $\mathbb{R}^9_+$, we obtain the following outcome:

$$\frac{dS}{dt}(S=0) = \mu N_h + \omega R > 0, \quad \frac{dV}{dt}(V=0) = \theta S > 0,$$
$$\frac{dI_s}{dt}(I_s=0) = \frac{p\beta_1}{N_h} SY + \frac{q\beta_3}{N_h} VY > 0, \quad \frac{dI_r}{dt}(I_r=0) = \frac{(1-p)\beta_2}{N_h} SY + \frac{(1-q)\beta_4}{N_h} VY > 0,$$
$$\frac{dI_{st}}{dt}(I_{st}=0) = \gamma I_s > 0, \quad \frac{dI_{rt}}{dt}(I_{rt}=0) = \delta I_r > 0, \quad \frac{dR}{dt}(R=0) = \tau V + \sigma I_{st} + \rho I_{rt} > 0,$$
$$\frac{dX}{dt}(X=0) = \eta N_v > 0, \quad \frac{dY}{dt}(Y=0) = \left(\frac{\beta_5}{N_h} I_s + \frac{\beta_6}{N_h} I_r\right) X > 0.$$

Because all directions along the boundary are nonnegative, every solution is directed inward toward $\mathbb{R}^9_+$. Consequently, if the initial condition is nonnegative within $\mathbb{R}^9_+$, the solution remains in this region for any time $t > 0$. This completes this proof. □

Having established the positivity of the state variables, we now prove that the model solutions are bounded from above. This ensures that the populations do not grow without bounds, thereby validating the well-posedness of the model within a realistic epidemiological context.

Theorem 2. *Let all model parameters in system* (1) *be nonnegative and the initial conditions be nonnegative and finite. Subsequently, the solutions of the malaria model* (1) *are bounded above for all* $t \geq 0$. *In particular, the total human population* $N_h(t)$ *and total mosquito population* $N_v(t)$ *satisfy*

$$N_h(t) = S(t) + V(t) + I_s(t) + I_r(t) + I_{st}(t) + I_{rt}(t) + R(t) \leq N_h, \quad \forall t \geq 0,$$

$$N_v(t) = X(t) + Y(t) \leq N_v, \quad \forall t \geq 0,$$

where N_h *and* N_v *are constants determined by initial conditions.*

Proof. Summing the equations for the human compartments in system (1) yields

$$\frac{dN_h}{dt} = \frac{dS}{dt} + \frac{dV}{dt} + \frac{dI_s}{dt} + \frac{dI_r}{dt} + \frac{dI_{st}}{dt} + \frac{dI_{rt}}{dt} + \frac{dR}{dt}.$$

Substituting from equations (1)(a)–(g), we find that all transition terms cancel, and only the recruitment and natural death terms remain:

$$\frac{dN_h}{dt} = \mu N_h - \mu(S + V + I_s + I_r + I_{st} + I_{rt} + R) = \mu N_h - \mu N_h = 0.$$

Therefore, the total human population remained constant.

$$N_h(t) = N_h(0) = N_h, \quad \forall t \geq 0.$$

Similarly, summing the equations for the mosquito compartments (1)(h)–(i) gives

$$\frac{dN_v}{dt} = \frac{dX}{dt} + \frac{dY}{dt} = \eta N_v - \eta N_v = 0.$$

Thus, the mosquito population was constant.

$$N_v(t) = N_v(0) = N_v, \quad \forall t \geq 0.$$

Because all compartment values are nonnegative (positivity has been assumed), and the total population is constant, it follows that each compartment is bounded above by the respective total population. That is,

$$0 \leq S(t), V(t), I_s(t), I_r(t), I_{st}(t), I_{rt}(t), R(t) \leq N_h,$$

$$0 \leq X(t), Y(t) \leq N_v,$$

for all $t \geq 0$. Therefore, the solutions were uniformly bounded. □

3. Equilibrium Points and Basic Reproduction Number

Analyzing the model of malaria transmission necessitates the identification of the nonendemic equilibrium point, which offers insights into periods of stability when malaria does not propagate within the population. The equilibrium point in model (1) under nonendemic conditions is ascertained by setting the malaria infection rates in both hosts and vectors to zero, resulting in

$$E_0 = (\overline{S}, \overline{V}, 0, 0, 0, 0, \overline{R}, \overline{X}, 0),$$

with

$$\overline{S} = \frac{(\tau+\mu)(\omega+\mu)N_h}{\mu^2 + (\omega+\tau+\theta)\mu + (\tau+\theta)\omega + \tau\theta},$$
$$\overline{V} = \frac{(\omega+\mu)\theta N_h}{\mu^2 + (\omega+\tau+\theta)\mu + (\tau+\theta)\omega + \tau\theta},$$
$$\overline{R} = \frac{\theta\mu N_h}{\mu^2 + (\omega+\tau+\theta)\mu + (\tau+\theta)\omega + \tau\theta},$$

$$\overline{X} = N_v.$$

The basic reproduction number, represented by $\mathscr{R}_0$, is a vital parameter for assessing the potential for disease transmission within a population. The determination of $\mathscr{R}_0$ is achieved using the next-generation matrix, which incorporates the Jacobian matrix of the infected subpopulations in relation to other subpopulations. The set of equations (1) was analyzed at the nonendemic equilibrium point (E_0).

$$F = \begin{bmatrix} 0 & 0 & 0 & 0 & \frac{p\beta_1(\tau+\mu)(\omega+\mu)+q\beta_3(\omega+\mu)\theta}{\mu^2+(\omega+\tau+\theta)\mu+(\tau+\theta)\omega+\tau\theta} & 0 \\ 0 & 0 & 0 & 0 & \frac{(1-p)\beta_2(\tau+\mu)(\omega+\mu)+(1-q)\beta_4(\omega+\mu)\theta}{\mu^2+(\omega+\tau+\theta)\mu+(\tau+\theta)\omega+\tau\theta} & 0 \\ 0 & 0 & 0 & 0 & 0 & 0 \\ 0 & 0 & 0 & 0 & 0 & 0 \\ \beta_5\frac{N_v}{N_h} & 0 & 0 & 0 & 0 & 0 \\ 0 & \beta_6\frac{N_v}{N_h} & 0 & 0 & 0 & 0 \end{bmatrix}$$

The Jacobian matrix pertaining to the infected subpopulation, which remains isolated from the other subpopulations upon entering the host or vector, is represented by the following matrix:

$$W = \begin{bmatrix} \gamma+\mu & 0 & 0 & 0 & 0 & 0 \\ 0 & \delta+\mu & 0 & 0 & 0 & 0 \\ -\gamma & 0 & \sigma+\mu & 0 & 0 & 0 \\ 0 & -\delta & 0 & \rho+\mu & 0 & 0 \\ 0 & 0 & 0 & 0 & \eta & 0 \end{bmatrix}$$

The basic reproduction number associated with system equation (1) is determined as the largest eigenvalue of the matrix FW^{-1} [26], represented as

$$R_{0v} = \sqrt{\frac{\beta_5 N_v(\delta+\mu)\left[p\beta_1(\tau+\mu)(\omega+\mu)+q\beta_3(\omega+\mu)\theta\right]+\beta_7+\beta_8}{(\delta+\mu)(\gamma+\mu)(\mu^2+(\omega+\tau+\theta)\mu+(\tau+\theta)\omega+\tau\theta)N_h}} \tag{2}$$

with

$$\beta_7 = \beta_6 N_v(\gamma+\mu)\left[(1-p)\beta_2(\tau+\mu)(\omega+\mu)\right], \quad \beta_8 = (1-q)\beta_4(\omega+\mu)\theta.$$

Having previously derived the basic reproduction number R_{0v} under the assumption that vaccination is incorporated into the model, we now consider a scenario in which vaccination is

absent. The basic reproduction number in the absence of vaccination is determined as follows:

$$R_0 = \sqrt{\frac{\beta_5 N_v(\delta+\mu)p\beta_1\mu(\omega+\mu)+\beta_6 N_v(\gamma+\mu)(1-p)\beta_2\mu(\omega+\mu)}{(\delta+\mu)(\gamma+\mu)(\mu^2+\omega\mu)N_h}} \tag{3}$$

A comparison of the expressions for R_0 and R_{0v} reveals that the numerator of R_0 is significantly larger than that of R_{0v}, whereas the denominator of R_0 is comparable or slightly smaller than that of R_{0v}. Thus, we have

$$R_0 > R_{0v}.$$

This analytical observation is further supported by numerical evaluation using the parameter values listed in Table 1, which yields

$$R_0 = 4.12173313 > 0.00394931 = R_{0v}$$

as expected.

This result clearly indicates that incorporating vaccination into the malaria transmission model substantially reduced the basic reproduction number. In other words, vaccination effectively lowers the potential for disease spread compared with scenarios in which vaccination is not implemented. This finding reinforces the conclusion drawn from the analysis of the nonendemic equilibrium and provides a strong justification for the inclusion of vaccination in malaria control strategies.

To assess the stability of the nonendemic equilibrium, we analyze the basic reproduction number R_{0v} derived earlier. This threshold parameter serves as a key indicator of whether the disease will persist or die in the population. The following theorem provides the condition under which the nonendemic equilibrium is locally asymptotically stable.

Theorem 3. *The nonendemic equilibrium of the system* (1) *is locally asymptotically stable if the basic reproduction number* $R_{0v} < 1$ *and unstable if* $R_{0v} > 1$.

Next, we study the local stability of nonendemic equilibrium of the system (1).

Proof. The Jacobian matrix of system (1) is

$$
J = \begin{bmatrix}
\left[-\left(\theta+\frac{p\beta_1}{N_h}Y+\frac{(1-p)\beta_2}{N_h}Y+\mu\right) \;\; 0 \;\; 0 \;\; 0 \;\; 0 \;\; 0 \;\; \omega \;\; 0 \;\; -\left(\frac{p\beta_1}{N_h}+\frac{(1-p)\beta_2}{N_h}\right)S\right] \\
\left[\theta \;\; -\left(\frac{q\beta_3}{N_h}Y+\frac{(1-q)\beta_4}{N_h}Y+\tau+\mu\right) \;\; 0 \;\; 0 \;\; 0 \;\; 0 \;\; 0 \;\; 0 \;\; -\left(\frac{q\beta_3}{N_h}+\frac{(1-q)\beta_4}{N_h}\right)V\right] \\
\left[\frac{p\beta_1}{N_h}Y \;\; \frac{q\beta_3}{N_h}Y \;\; -(\gamma+\mu) \;\; 0 \;\; 0 \;\; 0 \;\; 0 \;\; 0 \;\; \frac{p\beta_1}{N_h}S+\frac{q\beta_3}{N_h}V\right] \\
\left[\frac{(1-p)\beta_2}{N_h}Y \;\; \frac{(1-q)\beta_4}{N_h}Y \;\; 0 \;\; -(\delta+\mu) \;\; 0 \;\; 0 \;\; 0 \;\; 0 \;\; \frac{(1-p)\beta_2}{N_h}S+\frac{(1-q)\beta_4}{N_h}V\right] \\
\left[0 \;\; 0 \;\; \gamma \;\; 0 \;\; -(\sigma+\mu) \;\; 0 \;\; 0 \;\; 0 \;\; 0\right] \\
\left[0 \;\; 0 \;\; 0 \;\; \delta \;\; 0 \;\; -(\rho+\mu) \;\; 0 \;\; 0 \;\; 0\right] \\
\left[0 \;\; \tau \;\; 0 \;\; 0 \;\; \sigma \;\; \rho \;\; -(\omega+\mu) \;\; 0 \;\; 0\right] \\
\left[0 \;\; 0 \;\; -\frac{\beta_5}{N_h}X \;\; -\frac{\beta_6}{N_h}X \;\; 0 \;\; 0 \;\; 0 \;\; -\left(\frac{\beta_5}{N_h}I_s+\frac{\beta_6}{N_h}I_r+\eta\right) \;\; 0\right] \\
\left[0 \;\; 0 \;\; \frac{\beta_5}{N_h}X \;\; \frac{\beta_6}{N_h}X \;\; 0 \;\; 0 \;\; 0 \;\; \left(\frac{\beta_5}{N_h}I_s+\frac{\beta_6}{N_h}I_r\right) \;\; -\eta\right]
\end{bmatrix} \tag{4}
$$

Let

$$
\begin{aligned}
\Delta &= \mu^2+(\omega+\tau+\theta)\mu+\omega(\tau+\theta)+\tau\theta, \\
B_1 &= \beta_1 p(\mu+\omega)(\mu+\tau)+\beta_3 q\theta(\mu+\omega), \\
B_2 &= \beta_2(1-p)(\mu+\omega)(\mu+\tau)+\beta_4(1-q)\theta(\mu+\omega), \\
B_3 &= \frac{\beta_5 N_v}{N_h}, \quad B_4 = \frac{\beta_6 N_v}{N_h}.
\end{aligned}
$$

Then, the Jacobian matrix evaluated at the nonendemic equilibrium E_0 is:

$$
J(E_0) = \begin{bmatrix}
-\mu-\theta & 0 & 0 & 0 & 0 & 0 & \omega & 0 & 0 \\
\theta & -\mu-\tau & 0 & 0 & 0 & 0 & 0 & 0 & 0 \\
0 & 0 & -\gamma-\mu & 0 & 0 & 0 & 0 & 0 & \frac{B_1}{\Delta} \\
0 & 0 & 0 & -\delta-\mu & 0 & 0 & 0 & 0 & \frac{B_2}{\Delta} \\
0 & 0 & \gamma & 0 & -\mu-\sigma & 0 & 0 & 0 & 0 \\
0 & 0 & 0 & \delta & 0 & -\mu-\rho & 0 & 0 & 0 \\
0 & \tau & 0 & 0 & \sigma & \rho & -\mu-\omega & 0 & 0 \\
0 & 0 & -B_3 & -B_4 & 0 & 0 & 0 & -\eta & 0 \\
0 & 0 & B_3 & B_4 & 0 & 0 & 0 & 0 & -\eta
\end{bmatrix}
$$

The first three eigenvalues are

$$\lambda_1 = -(\gamma+\mu), \quad \lambda_2 = -(\mu+\sigma), \quad \lambda_3 = -\eta,$$

$$\lambda_{4,5} = \frac{1}{2}\left(-(\delta+\mu+\eta) \pm \sqrt{(\delta+\mu+\eta)^2 - 4\left[(\delta+\mu)\eta - \frac{B_1B_4}{\Delta}\right]}\right),$$

and the next two eigenvalues form the characteristic equation below

$$p(\lambda) = \lambda^2 + a_1\lambda + a_2 = 0, \tag{5}$$

where

$$a_1 = \delta+\mu+\eta, \quad a_2 = (\delta+\mu)\eta - \frac{B_1B_4}{\Delta},$$

and the remaining four eigenvalues form the following characteristic equation

$$p(\lambda) = \lambda^4 + b_1\lambda^3 + b_2\lambda^2 + b_3\lambda + b_4 = 0, \tag{6}$$

where

$$b_1 = 4\mu + \theta + \tau + \omega + \rho,$$

$$b_2 = (\mu+\theta)(\mu+\tau) + (2\mu+\theta+\tau)(2\mu+\omega+\rho) + (\mu+\omega)(\mu+\rho),$$

$$b_3 = (\mu+\theta)(\mu+\tau)(2\mu+\omega+\rho) + (2\mu+\theta+\tau)(\mu+\omega)(\mu+\rho),$$

$$b_4 = (\mu+\theta)(\mu+\tau)(\mu+\omega)(\mu+\rho) + \omega\theta\tau.$$

The Routh-Hurwitz criteria to guarantee the real part of all eigenvalues in (5) and (6) are negative, is given as follows

$$(i)\, a_1 > 0, \quad (ii)\, a_2 > 0,$$

and

$$(iii)\, b_1 > 0, \quad (iv)\, b_4 > 0, \quad (v)\, b_1b_2 - b_3 > 0, \quad (vi)\, (b_1b_2 - b_3)b_3 - b_1^2b_4 > 0,$$

respectively.

Clearly, a_1, b_1, and b_4 were positive. In the cases of (v) and (vi), both long expressions can be expanded and guaranteed to be positive. For the case of $a(ii)$, we have $a_2 > 0$ if and only if

$$R_{0v} = \frac{B_1B_4}{\Delta(\delta+\mu)\eta} < 1.$$

□

Theorem 4. *Let $R_{0v} < 1$. Then the disease-free equilibrium point E_0 is globally asymptotically stable within the biologically feasible region*

$$\Omega = \left\{ X \in \mathbb{R}^9_+ \,\middle|\, S+V+I_s+I_r+I_{st}+I_{rt}+R \le N_h,\ X+Y \le N_v \right\},$$

where N_h and N_v denote the total populations of humans and vectors (mosquitoes), respectively.

Proof. To establish the global asymptotic stability of the disease-free equilibrium E_0, we construct a Lyapunov function of the form

$$\mathscr{L}(t) = a_1 I_s + a_2 I_r + a_3 I_{st} + a_4 I_{rt} + a_5 Y,$$

where $a_1, a_2, a_3, a_4, a_5 > 0$ are positive constants to be determined. Taking the time derivative of $\mathscr{L}(t)$ along the trajectories of the system yields

$$\frac{d\mathscr{L}(t)}{dt} = a_1 \left(\frac{p\beta_1 SY}{N_h} + \frac{q\beta_3 VY}{N_h} - (\gamma+\mu) I_s \right) + a_2 \left(\frac{(1-p)\beta_2 SY}{N_h} + \frac{(1-q)\beta_4 VY}{N_h} - (\delta+\mu) I_r \right)$$
$$+ \quad a_3 (\gamma I_s - (\sigma+\mu) I_{st}) + a_4 (\delta I_r - (\rho+\mu) I_{rt}) + a_5 \left(\left(\frac{\beta_5 I_s + \beta_6 I_r}{N_h} \right) X - \eta Y \right).$$

To ensure that $\frac{d\mathscr{L}(t)}{dt} \le 0$ for all $X \in \Omega$, we choose the coefficients a_i to satisfy the following inequalities:

$$a_1(\gamma+\mu) > a_3\gamma + \frac{a_5\beta_5 X}{N_h}, \quad a_2(\delta+\mu) > a_4\delta + \frac{a_5\beta_6 X}{N_h}, \quad a_3(\sigma+\mu) > 0, \quad a_4(\rho+\mu) > 0,$$

$$a_5\eta > a_1 \left(\frac{p\beta_1 \bar{S}}{N_h} + \frac{q\beta_3 \bar{V}}{N_h} \right) + a_2 \left(\frac{(1-p)\beta_2 \bar{S}}{N_h} + \frac{(1-q)\beta_4 \bar{V}}{N_h} \right),$$

where $\bar{S}$ and $\bar{V}$ denote the maximum values of the susceptible human and vector populations, respectively, within the domain Ω.

Under these conditions, the derivative $\frac{d\mathscr{L}(t)}{dt}$ is negative definite in Ω except on the invariant set where $I_s = I_r = I_{st} = I_{rt} = Y = 0$. Consequently, we define an equivalent Lyapunov function:

$$\mathscr{L}(t) = a_1 I_s + a_2 I_r + \frac{a_1\gamma}{\sigma+\mu} I_{st} + \frac{a_2\delta}{\rho+\mu} I_{rt} + a_5 Y,$$

with $a_1, a_2 > 0$ and a_5 sufficiently large such that $\frac{d\mathscr{L}(t)}{dt} \le 0$.

According to LaSalle's Invariance Principle [27, 28], all trajectories initiated in Ω approach the largest invariant set, where $\frac{d\mathscr{L}(t)}{dt} = 0$, which corresponds to disease-free equilibrium E_0. Therefore, E_0 is globally asymptotically stable in Ω. □

To determine the endemic equilibrium of the system (1), we consider the steady-state condition in which the disease persists within the population. This implies that the time derivatives are all set to zero and the infected compartments satisfy $I_s^* > 0$, $I_r^* > 0$, and $Y^* > 0$. Let the endemic equilibrium be denoted by

$$E^* = (S^*, V^*, I_s^*, I_r^*, I_{st}^*, I_{rt}^*, R^*, X^*, Y^*).$$

From the steady-state equations for the treated human compartments, we obtain

$$I_{st}^* = \frac{\gamma}{\sigma+\mu} I_s^*,$$
$$I_{rt}^* = \frac{\delta}{\rho+\mu} I_r^*.$$

Substituting the expressions for I_{st}^* and I_{rt}^* into the equation for the recovered class R, we get

$$R^* = \frac{1}{\omega+\mu}\left(\tau V^* + \frac{\gamma\sigma}{\sigma+\mu} I_s^* + \frac{\delta\rho}{\rho+\mu} I_r^*\right).$$

Next, define the force of infection from humans to mosquitoes as

$$\Lambda_h = \frac{\beta_5}{N_h} I_s^* + \frac{\beta_6}{N_h} I_r^*.$$

Then, the mosquito population at equilibrium satisfies

$$X^* = \frac{\eta N_v}{\Lambda_h + \eta},$$
$$Y^* = \frac{\Lambda_h}{\eta} X^* = \frac{\Lambda_h N_v}{\Lambda_h + \eta}.$$

The equilibrium values for the infected human compartments were obtained using the following equation:

$$I_s^* = \frac{1}{\gamma+\mu}\left(\frac{p\beta_1}{N_h} S^* Y^* + \frac{q\beta_3}{N_h} V^* Y^*\right),$$
$$I_r^* = \frac{1}{\delta+\mu}\left(\frac{(1-p)\beta_2}{N_h} S^* Y^* + \frac{(1-q)\beta_4}{N_h} V^* Y^*\right).$$

By substituting Y^*, I_s^*, I_r^*, and R^* into the equilibrium equations for S and V, the system is reduced to two nonlinear equations:

$$0 = \mu N_h - \left(\theta + \frac{p\beta_1 + (1-p)\beta_2}{N_h} Y^* + \mu\right) S^* + \omega R^*,$$

$$0 = \theta S^* - \left(\frac{q\beta_3 + (1-q)\beta_4}{N_h} Y^* + \tau + \mu \right) V^*.$$

These equations are implicitly coupled through nonlinear expressions for Y^*, I_s^*, I_r^*, and R^*, and thus cannot be solved analytically in a closed form. Instead, a numerical solution was used.

4. MALARIA CONTROL

The malaria control strategies considered in this study are defined as follows. First, *preventive control*, denoted by $u_1(t)$, involves the use of insecticide-treated bed nets at night to minimize contact between susceptible and infected female mosquitoes. Second, *vaccination control*, represented by $u_2(t)$, focuses on enhancing the effectiveness of vaccination by administering supplementary treatments such as multivitamins. Third, *treatment control*, denoted by $u_3(t)$, aims to improve treatment outcomes through community-based educational programs that emphasize adherence to antimalarial medications and healthy lifestyle practices.

These control measures are incorporated into the model dynamics, as represented by the controlled system of equations (7), which modifies the original malaria transmission model (1) by integrating time-dependent control functions.

$$\frac{dS}{dt} = \mu N_h - \left(\theta + \frac{p\beta_1(1-u_1)}{N_h} Y + \frac{(1-p)\beta_2(1-u_1)}{N_h} Y + \mu \right) S + \omega R, \tag{7a}$$

$$\frac{dV}{dt} = \theta S - \left(\frac{q\beta_3}{N_h} Y + \frac{(1-q)\beta_4}{N_h} Y + \tau(1+u_2) + \mu \right) V, \tag{7b}$$

$$\frac{dI_s}{dt} = \frac{p\beta_1(1-u_1)}{N_h} SY + \frac{q\beta_3}{N_h} VY - (\gamma+\mu) I_s, \tag{7c}$$

$$\frac{dI_r}{dt} = \frac{(1-p)\beta_2(1-u_1)}{N_h} SY + \frac{(1-q)\beta_4}{N_h} VY - (\delta+\mu) I_r, \tag{7d}$$

$$\frac{dI_{st}}{dt} = \gamma I_s - (\sigma(1+u_3)+\mu) I_{st}, \tag{7e}$$

$$\frac{dI_{rt}}{dt} = \delta I_r - (\rho(1+u_3)+\mu) I_{rt}, \tag{7f}$$

$$\frac{dR}{dt} = \tau(1+u_2)V + \sigma(1+u_3) I_{st} + \rho(1+u_3) I_{rt} - (\omega+\mu) R, \tag{7g}$$

$$\frac{dX}{dt} = \eta N_v - \left(\frac{\beta_5}{N_h} I_s + \frac{\beta_6}{N_h} I_r + \eta \right) X, \tag{7h}$$

$$\frac{dY}{dt} = \left(\frac{\beta_5}{N_h} I_s + \frac{\beta_6}{N_h} I_r \right) X - \eta Y. \tag{7i}$$

In the controlled system of equations (7), control variables u_1, u_2, and u_3 are introduced to regulate the spread of malaria by targeting specific intervention strategies. To determine the optimal levels of these controls over time, the following objective function is formulated:

$$J(u_1,u_2,u_3) = \int_{t_0}^{t_f} \left(A_1 I_s + A_2 I_r + A_3 I_{st} + A_4 I_{rt} + C_1 u_1^2 + C_2 u_2^2 + C_3 u_3^2\right) dt, \tag{8}$$

where A_1, A_2, A_3, A_4 are nonnegative weighting parameters that reflect the relative importance of minimizing the populations of untreated and treated infected individuals, namely, I_s, I_r, I_{st}, and I_{rt}, respectively. The constants C_1, C_2, C_3 represent the relative costs associated with implementing controls u_1, u_2, and u_3, respectively. The goal is to minimize both the disease burden and intervention costs over the time horizon $[t_0, t_f]$.

To derive the necessary conditions for optimal control, we applied the Pontryagin Maximum Principle, as detailed in [3]. According to this principle, the Hamiltonian function is constructed by combining the integrand of the objective functional with the inner product of the adjoint variables and the state equations. The resulting Hamiltonian is given by

$$\begin{aligned}
H = {} & A_1 I_s + A_2 I_r + A_3 I_{st} + A_4 I_{rt} + C_1 u_1^2 + C_2 u_2^2 + C_3 u_3^2 \\
& + \lambda_1 \left(\mu N_h + \omega R - \theta S - \frac{p\beta_1 (1-u_1) SY}{N_h} - \frac{(1-p)\beta_2 (1-u_1) SY}{N_h} - \mu S \right) \\
& + \lambda_2 \left(\theta S - \psi V - \mu (1+u_2) V \right) \\
& + \lambda_3 \left(\frac{p\beta_1 (1-u_1) SY}{N_h} + \psi V - (\gamma + \mu) I_s \right) \\
& + \lambda_4 \left(\frac{(1-p)\beta_2 (1-u_1) SY}{N_h} + \psi V - (\delta + \mu) I_r \right) \\
& + \lambda_5 \left(\gamma I_s - (\sigma (1+u_3) + \mu) I_{st} \right) \\
& + \lambda_6 \left(\delta I_r - (\rho (1+u_3) + \mu) I_{rt} \right) \\
& + \lambda_7 \left(\tau (1+u_2) V + \sigma I_{st} + \rho I_{rt} - (\omega + \mu) R \right) \\
& + \lambda_8 \left(\eta - \frac{\beta_5 I_s X}{N_h} - \frac{\beta_6 I_r X}{N_h} - \mu X \right) \\
& + \lambda_9 \left(\frac{\beta_5 I_s X}{N_h} + \frac{\beta_6 I_r X}{N_h} - \eta Y \right),
\end{aligned} \tag{9}$$

where λ_i for $i = 1,2,\ldots,9$ are adjoint (co-state) variables associated with each state variable. The Hamiltonian expression in Equation (9) forms the foundation for establishing the necessary optimality conditions and proving the existence of optimal controls for the system (7).

Theorem 5. *There exists an optimal control* $u^* = (u_1^*, u_2^*, u_3^*) \in \Omega$ *such that*

$$J(u_1^*, u_2^*, u_3^*) = \min_{(u_1,u_2,u_3)\in\Omega} J(u_1, u_2, u_3). \tag{10}$$

Proof. The controlled system (7) is governed by bounded state variables and admissible controls u_1, u_2, u_3 that are assumed to lie within a closed and convex set $\Omega \subset [0,1]^3$. Furthermore, the right-hand side of each equation in the system is continuous and satisfies the Lipschitz condition with respect to the state variables, thereby ensuring the existence and uniqueness of the solutions.

The objective functional $J(u_1, u_2, u_3)$ given in (8) is convex in the control variables and is composed of a linear combination of state variables and quadratic control terms. This convexity, combined with the boundedness of the state solutions and the compactness of the admissible control set Ω, guarantees a lower semi-continuity of J.

Let ζ_1, ζ_2 be positive constants, and $\kappa > 1$. Then $J(u_1, u_2, u_3)$ can be bounded below by

$$J(u_1, u_2, u_3) \geq \zeta_1(|u_1|^2 + |u_2|^2 + |u_3|^2)^\kappa - \zeta_2,$$

to ensure coercivity of the functional.

Therefore, by the standard results in optimal control theory (see, e.g., [29]), the existence of an optimal control $u^* \in \Omega$ that minimizes the objective functional J is guaranteed. □

By applying the Hamiltonian function of equation (9), the adjoint function of state equation (7) is obtained according to Theorem 3.

Theorem 6. *Let the optimal controls* u_1, u_2, u_3 *satisfy the system of equations in* (10)*. The corresponding system of adjoint differential equations is then obtained for the state equation* (7)*:*

$$\begin{aligned}
\frac{d\lambda_1}{dt} &= (\lambda_1 - \lambda_2)\theta + \frac{(\lambda_1 - \lambda_3)p\beta_1(1-u_1)Y}{N_h} + \frac{(\lambda_1 - \lambda_4)(1-p)\beta_2(1-u_1)Y}{N_h} + \mu\lambda_1,\\
\frac{d\lambda_2}{dt} &= \frac{(\lambda_2 - \lambda_3)q\beta_3 Y}{N_h} + \frac{(\lambda_2 - \lambda_4)(1-q)\beta_4 Y}{N_h} + (\lambda_2 - \lambda_7)\tau(1+u_2) + \mu\lambda_2,\\
\frac{d\lambda_3}{dt} &= -A_1 + (\lambda_3 - \lambda_5)\gamma + \mu\lambda_3,
\end{aligned}$$

$$\begin{aligned}
\frac{d\lambda_4}{dt} &= -A_2 + (\lambda_4 - \lambda_6)\delta + \mu\lambda_4, \\
\frac{d\lambda_5}{dt} &= -A_3 + (\lambda_5 - \lambda_7)\sigma(1+u_3) + \mu\lambda_5, \\
\frac{d\lambda_6}{dt} &= -A_4 + (\lambda_6 - \lambda_7)\rho(1+u_3) + \mu\lambda_6, \\
\frac{d\lambda_7}{dt} &= (\lambda_7 - \lambda_1)\omega + \mu\lambda_7, \\
\frac{d\lambda_8}{dt} &= -\frac{(\lambda_3 - \lambda_4)(\beta_5 I_s + \beta_6 I_r)}{N_h} + \eta\lambda_8, \\
\frac{d\lambda_9}{dt} &= \frac{(\lambda_1 - \lambda_3)p\beta_1(1-u_1)S + (\lambda_2 - \lambda_4)(1-p)\beta_2(1-u_1)S}{N_h} + \frac{(\lambda_3 - \lambda_4)(\beta_3 + (1-q)\beta_4)}{N_h} \\
&\quad + \eta\lambda_9. \qquad (11)
\end{aligned}$$

with the transversality condition

$$\lambda_i(t_f) = 0, \quad \textit{for } i = 1,2,\ldots,9,$$

and the optimal control values u_1^*, u_2^*, u_3^* are given by

$$u_1^* = \min\left\{1, \max\left[0, \frac{(\lambda_3 - \lambda_4)\beta_1 SY + (\lambda_4 - \lambda_1)(1-p)\beta_2 SY}{2C_1 N_h}\right]\right\}, \qquad (12)$$

$$u_2^* = \min\left\{1, \max\left[0, \frac{(\lambda_2 - \lambda_7)\tau V}{2C_2}\right]\right\}, \qquad (13)$$

$$u_3^* = \min\left\{1, \max\left[0, \frac{(\lambda_5 - \lambda_7)\sigma I_{st} + (\lambda_6 - \lambda_7)\rho I_{rt}}{2C_3}\right]\right\}. \qquad (14)$$

Proof. Based on the state equation (7), we derive a system of adjoint equations that corresponds to the system of state equations:

$$S, V, I_s, I_r, I_{st}, I_{rt}, R, X, Y$$

as follows:

$$\lambda_1' = -\frac{\partial H}{\partial S} = (\lambda_1 - \lambda_2)\theta + \frac{(\lambda_1 - \lambda_3)p\beta_1(1-u_1)Y}{N_h} + \cdots$$

$$\begin{aligned}
\lambda_1' &= (\lambda_1 - \lambda_2)\theta + \frac{(\lambda_1 - \lambda_3)p\beta_1(1-u_1)Y}{N_h} + \frac{(\lambda_1 - \lambda_4)(1-p)\beta_2(1-u_1)Y}{N_h} + \mu\lambda_1, \\
\lambda_2' &= \frac{(\lambda_2 - \lambda_3)q\beta_3 Y}{N_h} + \frac{(\lambda_2 - \lambda_4)(1-q)\beta_4 Y}{N_h} + (\lambda_2 - \lambda_7)\tau(1+u_2) + \mu\lambda_2, \\
\lambda_3' &= -A_1 + (\lambda_3 - \lambda_5)\gamma + \mu\lambda_3,
\end{aligned}$$

$$\lambda_4' = -A_2 + (\lambda_4 - \lambda_6)\delta + \mu\lambda_4,$$

$$\lambda_5' = -A_3 + (\lambda_5 - \lambda_7)\sigma(1+u_3) + \mu\lambda_5,$$

$$\lambda_6' = -A_4 + (\lambda_6 - \lambda_7)\rho(1+u_3) + \mu\lambda_6,$$

$$\lambda_7' = (\lambda_7 - \lambda_1)\omega + \mu\lambda_7,$$

$$\lambda_8' = -\frac{(\lambda_3 - \lambda_4)(\beta_5 + \beta_6)I_r}{N_h} + \eta\lambda_8,$$

$$\lambda_9' = \frac{(\lambda_1 - \lambda_3)(1-u_1)Sp\beta_1 + (\lambda_1 - \lambda_4)(1-u_1)S(1-p)\beta_2}{N_h} + \frac{(\lambda_2 - \lambda_4)(\beta_3 + (1-q)\beta_4)}{N_h} + \eta\lambda_9.$$

Based on the system of equations (9), the optimal control is obtained u_1^*, u_2^*, u_3^* as follows:

$$\frac{\partial H}{\partial u_1} = 0 \Rightarrow u_1 = \frac{(\lambda_3 - \lambda_4)p\beta_1 SY + (\lambda_4 - \lambda_1)(1-p)\beta_2 SY}{2C_1 N_h},$$

$$\frac{\partial H}{\partial u_2} = 0 \Rightarrow u_2 = \frac{(\lambda_2 - \lambda_7)\tau V}{2C_2},$$

$$\frac{\partial H}{\partial u_3} = 0 \Rightarrow u_3 = \frac{(\lambda_5 - \lambda_7)\sigma I_{st} + (\lambda_6 - \lambda_7)\rho I_{rt}}{2C_3}.$$

By imposing constraints on the controls, a comprehensive control description can be derived, as follows:

$$u_1^* = \begin{cases} 0, & \text{if } u_1 \leq 0, \\ \frac{(\lambda_3 - \lambda_4)p\beta_1 SY + (\lambda_4 - \lambda_1)(1-p)\beta_2 SY}{2C_1 N_h}, & \text{if } 0 < u_1 < 1, \\ 1, & \text{if } u_1 \geq 1, \end{cases}$$

$$u_2^* = \begin{cases} 0, & \text{if } u_2 \leq 0, \\ \frac{(\lambda_2 - \lambda_7)\tau V}{2C_2}, & \text{if } 0 < u_2 < 1, \\ 1, & \text{if } u_2 \geq 1, \end{cases}$$

$$u_3^* = \begin{cases} 0, & \text{if } u_3 \leq 0, \\ \frac{(\lambda_5 - \lambda_7)\sigma I_{st} + (\lambda_6 - \lambda_7)\rho I_{rt}}{2C_3}, & \text{if } 0 < u_3 < 1, \\ 1, & \text{if } u_3 \geq 1. \end{cases}$$

In accordance with the above expression, the optimal control is given by:

$$u_1^* = \min\left\{1, \max\left[0, \frac{(\lambda_3-\lambda_4)p\beta_1 SY + (\lambda_4-\lambda_1)(1-p)\beta_2 SY}{2C_1 N_h}\right]\right\},$$

$$u_2^* = \min\left\{1, \max\left[0, \frac{(\lambda_2-\lambda_7)\tau V}{2C_2}\right]\right\},$$

$$u_3^* = \min\left\{1, \max\left[0, \frac{(\lambda_5-\lambda_7)\sigma I_{st} + (\lambda_6-\lambda_7)\rho I_{rt}}{2C_3}\right]\right\},$$

□

5. NUMERICAL SIMULATION

The numerical simulations were initialized using the following initial population sizes:

$$S(0) = 1{,}700{,}000, \quad V(0) = 200{,}000, \quad I_s(0) = 45{,}000, \quad I_r(0) = 25{,}000,$$
$$I_{st}(0) = 17{,}000, \quad I_{rt}(0) = 6{,}000, \quad R(0) = 7{,}000, \quad X(0) = 3{,}000{,}000, \quad Y(0) = 100{,}000.$$

Figure 2 illustrates the numerical simulation of the malaria transmission model using the aforementioned initial conditions and the parameter values provided in Table 1. The susceptible (S) and vaccinated (V) compartments declined rapidly owing to exposure to infectious mosquitoes and subsequent transitions into infected classes. In contrast, both drug-sensitive (I_s) and drug-resistant (I_r) infected populations initially increased, reflecting active transmission in the early phase. Over time, these compartments peak and then decline as individuals transition into treatment compartments (I_{st} and I_{rt}), which exhibit sustained growth owing to ongoing treatment influx. The recovered population (R) increased during the early epidemic phase but gradually decreased owing to resusceptibility and natural death. Vector populations (X and Y) respond dynamically, with infected mosquitoes (Y) initially rising as they acquire infection from human hosts, while susceptible mosquitoes (X) decline and later recover owing to recruitment. These dynamics confirm the capacity of the model to capture essential features of malaria transmission and suggest the need for early intervention to curb the outbreak.

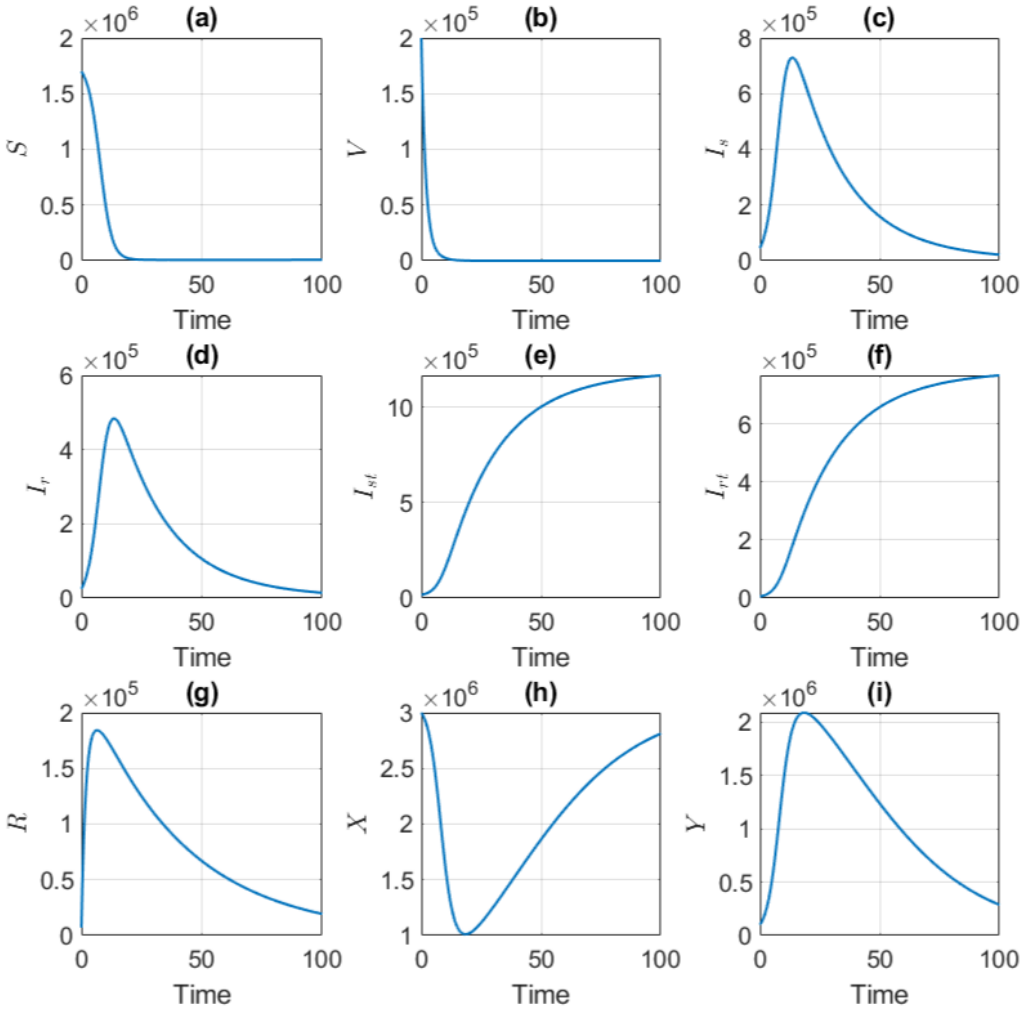

FIGURE 2. Time evolution of the malaria transmission model compartments (1). Each subplot (a)–(i) corresponds to one of the nine state variables: $S, V, I_s, I_r, I_{st}, I_{rt}, R, X, Y$, respectively.

We conducted a local sensitivity analysis using the elasticity index (EI) to examine how small perturbations in the individual parameters affect the basic reproduction number. This approach evaluates the relative contribution of each parameter to the changes in R_{0v} by measuring the proportional change in R_{0v} resulting from a proportional change in the parameter value. The analysis was performed using the baseline parameter values listed in Table 1. EI is defined as follows

$$EI = \frac{\partial R_{0v}}{\partial\, parameter} \times \frac{parameter}{R_{0v}}.$$

The results in Figure 3 indicate that the transmission rates from mosquitoes to susceptible humans (β_1) and from infected sensitive individuals to mosquitoes (β_5) have the highest positive elasticity indices, suggesting that vector-host transmission pathways are the most influential drivers of malaria spread. By contrast, the treatment rate of drug-sensitive infected individuals (γ) exhibited the most negative elasticity, implying that an increase in treatment effectiveness could substantially reduce the basic reproduction number R_{0v}. Other parameters, such as the proportion of individuals exposed to the sensitive strain (p) and the proportion of vaccinated individuals exposed to the sensitive strain (q), display moderate positive elasticity, signifying their notable but secondary impact on transmission dynamics. Parameters including the natural death rate (μ), resusceptibility rate (ω), vaccination rate (θ), and other treatment-related parameters (δ, τ) showed relatively small elasticity values, indicating a limited marginal influence under baseline conditions. These findings underscore the importance of targeting mosquito-human transmission efficiency and treatment coverage, particularly for drug-sensitive infections, in the development of effective malaria control strategies.

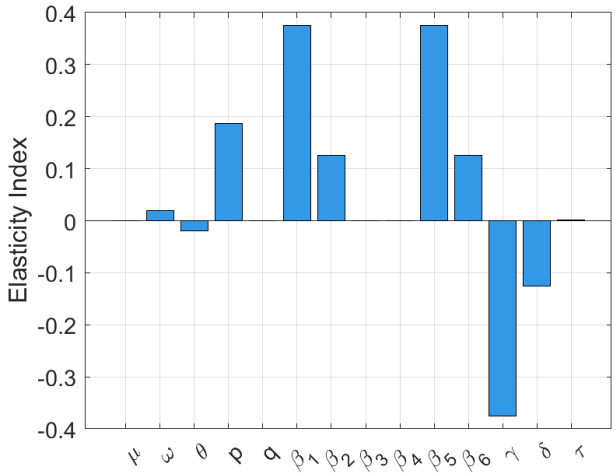

FIGURE 3. Bar plot of elasticity indices of the basic reproduction number R_{0v} with respect to selected model parameters. The results indicate that β_1 and β_5 have the strongest positive influence on R_{0v}, while β_6 exhibits the most negative effect.

Figure 4 presents contour plots of the basic reproduction number R_{0v} as a function of the most influential parameters identified through elasticity index analysis: the transmission rates from mosquitoes to susceptible humans (β_1) and from infected humans to mosquitoes (β_5), and the

treatment rate of drug-sensitive infections (γ). In panel (a), R_{0v} increases monotonically with both β_1 and β_5, confirming their synergistic role in amplifying malaria transmission through the vector-human cycle. Panel (b) illustrates the interaction between β_1 and γ, showing that increasing the treatment rate γ leads to a significant reduction in R_{0v}, particularly when the transmission is high. Similarly, Panel (c) demonstrates that increasing γ can effectively reduce R_{0v}, even in the presence of elevated values of β_5. These findings emphasize the importance of reducing vector-to-human transmission and enhancing treatment effectiveness in strategies aimed at suppressing malaria outbreaks.

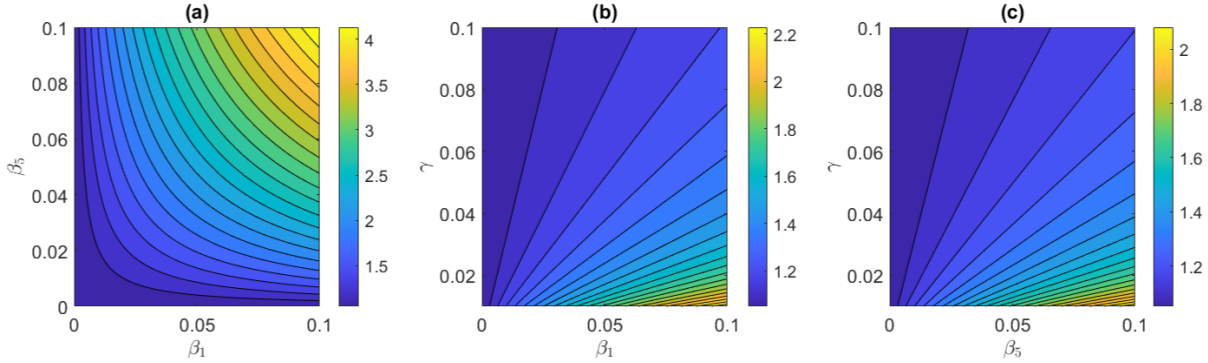

FIGURE 4. Contour plots of the basic reproduction number R_{0v} with respect to the most influential parameters based on elasticity analysis: (a) $R_{0v}(\beta_1, \beta_5)$, (b) $R_{0v}(\beta_1, \gamma)$, and (c) $R_{0v}(\beta_5, \gamma)$.

Pontryagin's Maximum Principle was employed to derive the optimal control strategy for the malaria transmission model governed by the system (7). The numerical implementation begins with an initial guess for the control variables, which are then utilized to solve the state system over the prescribed time horizon. The state equations are integrated forward in time using a fourth-order Runge–Kutta scheme, ensuring both accuracy and stability in approximating system dynamics.

Consistent with the transversality conditions outlined in equation (11), the adjoint equations are solved *backward* in time using the fourth-order Runge–Kutta method, incorporating previously computed state trajectories. The control functions are subsequently updated via a convex combination of the control values from the preceding iteration and those obtained from the characterization in Equation (10). This iterative procedure is repeated until convergence, which is defined as the point at which the differences between successive approximations of the control and state variables fall below a prescribed tolerance, as discussed in [3].

A numerical investigation was conducted to assess the efficacy of various malaria prevention and treatment strategies under different control scenarios. These scenarios include the application of individual control measures, pairwise combinations of two controls, and simultaneous implementation of all three control strategies. The simulation results were analyzed and compared systematically to evaluate the relative effectiveness of each intervention scheme in reducing malaria transmission.

The administrative costs associated with the infected subpopulations are incorporated into the objective functional through weighting constants A_1, A_2, A_3, A_4, which correspond to the populations I_s, I_r, I_{st}, I_{rt}. These weights reflect the relative burden of managing each infected group and are assigned as follows:

$$A_1 = 10, \quad A_2 = 10, \quad A_3 = 20, \quad A_4 = 20.$$

Similarly, the implementation costs of the control strategies u_1, u_2, u_3, representing the prevention and treatment measures, are captured by the constants C_1, C_2, C_3. These cost parameters were set uniformly as follows:

$$C_1 = 30, \quad C_2 = 30, \quad C_3 = 30.$$

The simulation results indicate that the number of individuals in the vaccinated compartment remains consistently lower under scenarios involving vaccination than under those without vaccination, as depicted in Figure 5.

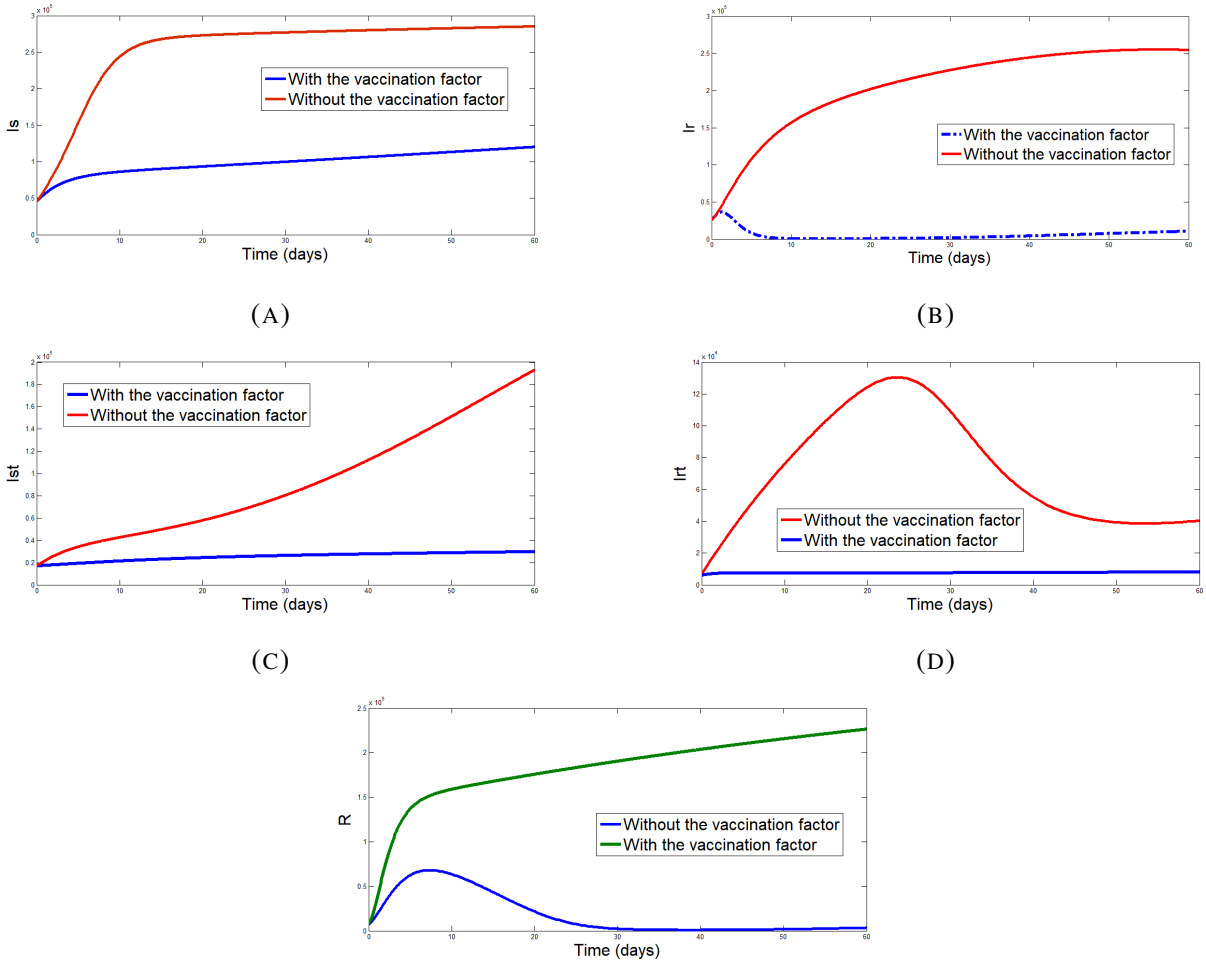

FIGURE 5. Time evolution of the human subpopulations under vaccination and non-vaccination scenarios: (a) drug-sensitive infected $I_s(t)$; (b) drug-resistant infected $I_r(t)$; (c) treated drug-sensitive infected $I_{st}(t)$; (d) treated drug-resistant infected $I_{rt}(t)$; (e) recovered individuals $R(t)$. Vaccination significantly reduces infection levels and enhances recovery.

Figure 5(a) illustrates that the implementation of vaccination leads to a substantial reduction in the number of individuals within the I_s compartment compared to the scenario without vaccination. In Figure 5(b), the I_r subpopulation exhibits rapid growth in the absence of vaccination. However, under the vaccination strategy, this subpopulation was eliminated by approximately $t = 10$ days. Furthermore, Figure 5(c) demonstrates that without vaccination, the I_{st} subpopulation undergoes a sharp increase, whereas with vaccination, its size remains stable over time.

Figure 5(d) shows that in the absence of vaccination, the I_{rt} subpopulation increases rapidly from the initial time to approximately $t = 23$ days, after which it begins to decline. By contrast, under the vaccination strategy, the I_{rt} compartment remained relatively stable throughout the simulation period. Finally, Figure 5(e) indicates that the number of individuals in the recovered compartment was consistently higher in the vaccination scenario than in the non-vaccination case, thereby confirming the effectiveness of vaccination in promoting recovery.

Figures 6(a) and (b) further demonstrate that the populations in the I_s and I_r compartments were significantly larger in the absence of control interventions. Among the individual control measures evaluated, control u_2 was notably more effective than u_1 in reducing the size of these infected compartments, underscoring its superior efficacy in mitigating malaria transmission.

Figures 6(c)–(d) reveal that the I_{st} and I_{rt} subpopulations experienced significant growth in the absence of control interventions. However, the combined implementation of controls u_1 and u_2 proved to be more effective at mitigating malaria transmission than scenarios without any control. Notably, control u_3, which targets the treatment, outperforms the combined effect of u_1 and u_2 in reducing the sizes of the I_{st} and I_{rt} compartments.

Figure 6(e) shows that applying control u_1 alone results in an increased number of individuals in the recovered compartment relative to the uncontrolled case. Nevertheless, the simultaneous application of controls u_1 and u_2 leads to a more substantial increase in the recovered population, highlighting the synergistic effect of combining the prevention strategies.

Figure 6(f) shows the control profiles over the simulation horizon. Control u_1, associated with preventive measures, was most effective during the early phase of the outbreak, particularly from the initial time up to $t = 12$ days. Control u_2 remains optimal from the beginning until

approximately $t = 27$ days. In contrast, control u_3, which focuses on treatment, continues to be the most effective strategy for reducing infection prevalence up to $t = 48$ days.

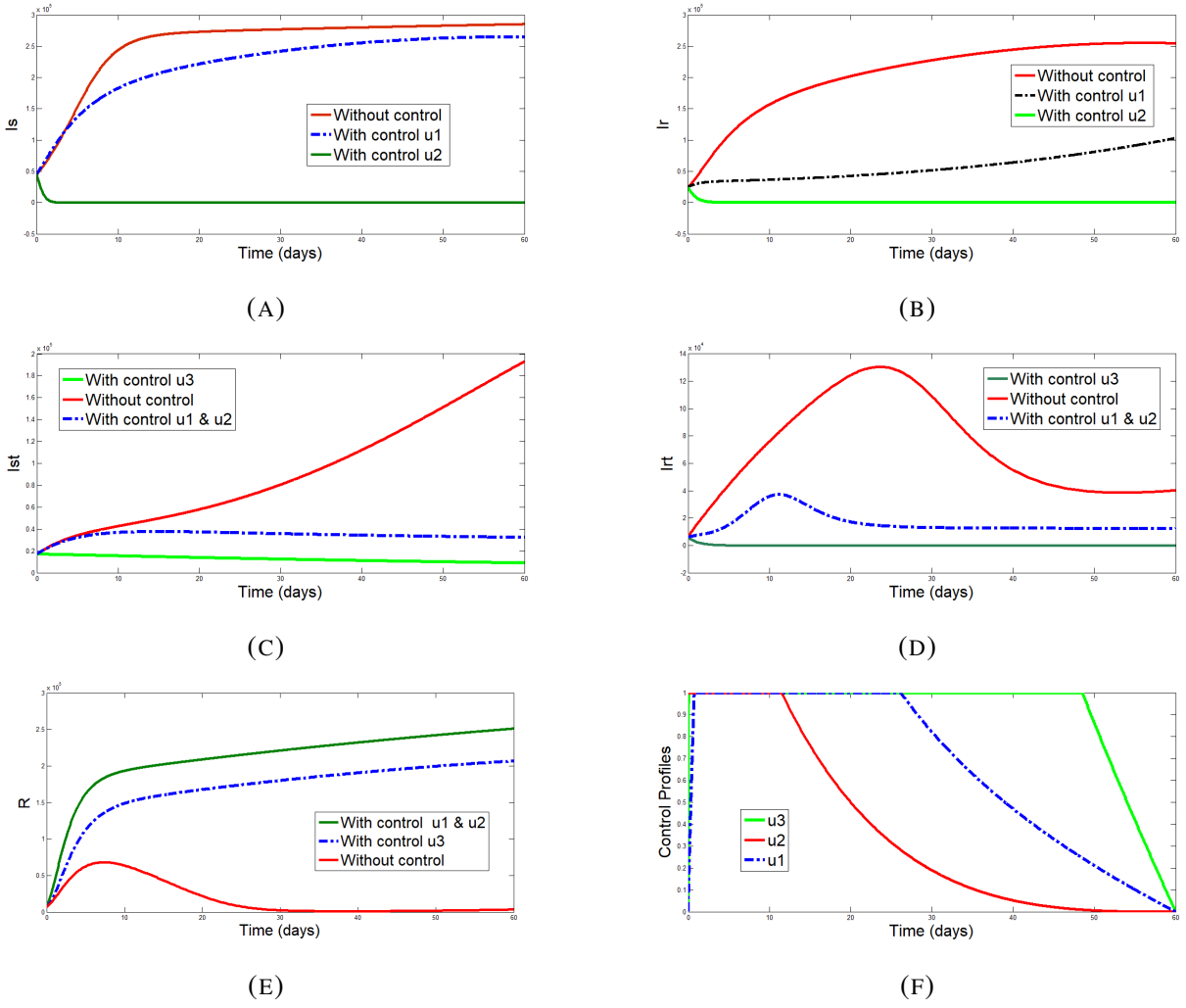

FIGURE 6. Dynamics of infected and recovered subpopulations under various control strategies: (a) drug-sensitive infected $I_s(t)$; (b) drug-resistant infected $I_r(t)$; (c) treated drug-sensitive infected $I_{st}(t)$; (d) treated drug-resistant infected $I_{rt}(t)$; (e) recovered individuals $R(t)$; (f) control profiles. Control strategies u_1, u_2, and u_3, individually or in combination, effectively reduce infection levels and enhance recovery compared to the uncontrolled scenario.

6. Discussion and Conclusion

This study developed and analyzed a compartmental model to investigate malaria transmission dynamics, incorporating the effects of vaccination and multiple control strategies. A central analytical finding was the derivation of the basic reproduction number in the presence of vaccination, which quantified the expected number of secondary infections generated by a single infected individual. It was shown that this reproduction number was lower when vaccination was included in the model, confirming that vaccination has the potential to substantially reduce disease spread. Furthermore, the stability analysis demonstrated that the disease-free equilibrium becomes locally asymptotically stable when the vaccination-adjusted reproduction number is less than one, reinforcing the importance of vaccine coverage in disease control.

Simulations of the temporal evolution of each compartment revealed important insights into the dynamics of malaria transmission. In the absence of interventions, the number of infected individuals increased sharply in both drug-sensitive and drug-resistant categories, whereas the susceptible and vaccinated populations declined rapidly. These dynamics illustrate how malaria can quickly spread within a population without control measures.

A local sensitivity analysis using the elasticity index highlighted the parameters that had the greatest influence on the reproduction number. The transmission rates from mosquitoes to susceptible individuals and from infected individuals to mosquitoes had the strongest positive influence, suggesting that vector-host interactions are the key drivers of malaria propagation. In contrast, the treatment rate of drug-sensitive infections had the strongest negative influence, indicating that enhancing the treatment effectiveness can significantly reduce transmission. Contour plots of the reproduction number further demonstrated how combinations of these key parameters shaped disease risk. Increasing treatment rates led to a clear reduction in transmission potential, even in the presence of high mosquito-human contact rates.

To evaluate the effectiveness of the intervention, an optimal control framework was applied using Pontryagin's Maximum Principle. The control strategies included preventive efforts such as bed net use, vaccination enhancement through auxiliary support, and treatment adherence campaigns. Numerical simulations showed that all three control strategies reduced the burden of infection, with vaccination and preventive efforts being particularly effective in reducing

new infections. Treatment-focused control was the most effective in decreasing the number of individuals in the treated infected classes and performed better than the other two controls when applied alone. Moreover, combining preventive and vaccination strategies yielded better outcomes than implementing either individually, but the treatment-based strategy still proved to be the most impactful when the goal was to minimize infection across all stages.

These results emphasize the synergistic benefits of combining vaccination with other treatment and preventive measures. The mathematical model illustrates how integrating multiple strategies can enhance the effectiveness of malaria-control programs. In particular, these findings support the continued development and deployment of malarial vaccines.

Future studies may extend this model by incorporating seasonality into mosquito dynamics, spatial heterogeneity, or age structure to better reflect real-world transmission patterns. Integrating parameter uncertainty and cost-effectiveness analysis would also enhance its applicability in public health decision-making.

ACKNOWLEDGEMENT

This study is supported by Kemendiktisaintek for Providing Grants of Penelitian Dasar BIMA 2025, through LPPM Universitas Cenderawasih.

CONFLICT OF INTERESTS

The authors declare that there is no conflict of interests.

REFERENCES

[1] WHO, World Malaria Report 2023, World Health Organization, (2023). https://www.who.int/teams/global-malaria-programme/reports/world-malaria-report-2023.

[2] N. Chitnis, J.M. Hyman, J.M. Cushing, Determining Important Parameters in the Spread of Malaria Through the Sensitivity Analysis of a Mathematical Model, Bull. Math. Biol. 70 (2008), 1272–1296. https://doi.org/10.1007/s11538-008-9299-0.

[3] S. Tchoumi, N. Njintang, J. Kamgang, J. Tchuenche, Malaria and Malnutrition in Children: a Mathematical Model, Frankl. Open 3 (2023), 100013. https://doi.org/10.1016/j.fraope.2023.100013.

[4] M. Sinan, H. Ahmad, Z. Ahmad, J. Baili, S. Murtaza, M. Aiyashi, T. Botmart, Fractional Mathematical Modeling of Malaria Disease with Treatment & Insecticides, Results Phys. 34 (2022), 105220. https://doi.org/10.1016/j.rinp.2022.105220.

[5] I. Faragó, R. Mosleh, Some Qualitative Properties of the Discrete Models for Malaria Propagation, Appl. Math. Comput. 439 (2023), 127628. https://doi.org/10.1016/j.amc.2022.127628.

[6] O. Collins, K. Duffy, A Mathematical Model for the Dynamics and Control of Malaria in Nigeria, Infect. Dis. Model. 7 (2022), 728–741. https://doi.org/10.1016/j.idm.2022.10.005.

[7] M. Karyana, L. Burdarm, S. Yeung, et al. Malaria Morbidity in Papua Indonesia, an Area with Multidrug Resistant Plasmodium Vivax and Plasmodium Falciparum, Malar. J. 7 (2008), 148. https://doi.org/10.1186/1475-2875-7-148.

[8] A.U. Rehman, R. Singh, J. Singh, Mathematical Analysis of Multi-Compartmental Malaria Transmission Model with Reinfection, Chaos Solitons Fractals 163 (2022), 112527. https://doi.org/10.1016/j.chaos.2022.112527.

[9] X. Jin, S. Jin, D. Gao, Mathematical Analysis of the Ross–macdonald Model with Quarantine, Bull. Math. Biol. 82 (2020), 47. https://doi.org/10.1007/s11538-020-00723-0.

[10] T. Song, C. Wang, B. Tian, Mathematical Models for Within-Host Competition of Malaria Parasites, Math. Biosci. Eng. 16 (2019), 6623–6653. https://doi.org/10.3934/mbe.2019330.

[11] J. Mohammed-Awel, A.B. Gumel, Mathematics of an Epidemiology-Genetics Model for Assessing the Role of Insecticides Resistance on Malaria Transmission Dynamics, Math. Biosci. 312 (2019), 33–49. https://doi.org/10.1016/j.mbs.2019.02.008.

[12] Fatmawati, F.F. Herdicho, Windarto, W. Chukwu, H. Tasman, An Optimal Control of Malaria Transmission Model with Mosquito Seasonal Factor, Results Phys. 25 (2021), 104238. https://doi.org/10.1016/j.rinp.2021.104238.

[13] E. Ndamuzi, P. Gahungu, Mathematical Modeling of Malaria Transmission Dynamics: Case of Burundi, J. Appl. Math. Phys. 09 (2021), 2447–2460. https://doi.org/10.4236/jamp.2021.910156.

[14] A.M. Niger, A.B. Gumel, Mathematical Analysis of the Role of Repeated Exposure on Malaria Transmission Dynamics, Differ. Equ. Dyn. Syst. 16 (2008), 251–287. https://doi.org/10.1007/s12591-008-0015-1.

[15] S. Olaniyi, M. Mukamuri, K. Okosun, O. Adepoju, Mathematical Analysis of a Social Hierarchy-Structured Model for Malaria Transmission Dynamics, Results Phys. 34 (2022), 104991. https://doi.org/10.1016/j.rinp.2021.104991.

[16] S.Y. Tchoumi, C.W. Chukwu, M.L. Diagne, H. Rwezaura, M.L. Juga, J.M. Tchuenche, Optimal Control of a Two-Group Malaria Transmission Model with Vaccination, Netw. Model. Anal. Health Inform. Bioinform. 12 (2022), 7. https://doi.org/10.1007/s13721-022-00403-0.

[17] P. Singh, B. Gor, K.H. Gazi, S. Mukherjee, A. Mahata, S.P. Mondal, Analysis and Interpretation of Malaria Disease Model in Crisp and Fuzzy Environment, Results Control. Optim. 12 (2023), 100257. https://doi.org/10.1016/j.rico.2023.100257.

[18] G. Adegbite, S. Edeki, I. Isewon, J. Emmanuel, T. Dokunmu, S. Rotimi, J. Oyelade, E. Adebiyi, Mathematical Modeling of Malaria Transmission Dynamics in Humans with Mobility and Control States, Infect. Dis. Model. 8 (2023), 1015–1031. https://doi.org/10.1016/j.idm.2023.08.005.

[19] J. Nainggolan, Fatmawati, Optimal Prevention and Treatment Control of Malaria Model With Resistance Drug, Int. J. Sci. Technol. Res. 8 (2019), 1767–1769.

[20] F. Al Basir, T. Abraha, Mathematical Modelling and Optimal Control of Malaria Using Awareness-Based Interventions, Mathematics 11 (2023), 1687. https://doi.org/10.3390/math11071687.

[21] B.D. Handari, R.A. Ramadhani, C.W. Chukwu, S.H.A. Khoshnaw, D. Aldila, An Optimal Control Model to Understand the Potential Impact of the New Vaccine and Transmission-Blocking Drugs for Malaria: a Case Study in Papua and West Papua, Indonesia, Vaccines 10 (2022), 1174. https://doi.org/10.3390/vaccines10081174.

[22] Fatmawati, U.D. Purwati, J. Nainggolan, Parameter Estimation and Sensitivity Analysis of Malaria Model, J. Phys.: Conf. Ser. 1490 (2020), 012039. https://doi.org/10.1088/1742-6596/1490/1/012039.

[23] M.T. White, P. Walker, S. Karl, M.W. Hetzel, T. Freeman, A. Waltmann, M. Laman, L.J. Robinson, A. Ghani, I. Mueller, Mathematical Modelling of the Impact of Expanding Levels of Malaria Control Interventions on Plasmodium Vivax, Nat. Commun. 9 (2018), 3300. https://doi.org/10.1038/s41467-018-05860-8.

[24] S. Tchoumi, M. Diagne, H. Rwezaura, J. Tchuenche, Malaria and Covid-19 Co-Dynamics: a Mathematical Model and Optimal Control, Appl. Math. Model. 99 (2021), 294–327. https://doi.org/10.1016/j.apm.2021.06.016.

[25] D. Aldila, A.H. Hassan, M.H.N. Aziz, P.Z. Kamalia, An Analytical Transmission Model for Evaluating Pneumonia Vaccination and Control Strategies, Healthc. Anal. 7 (2025), 100394. https://doi.org/10.1016/j.health.2025.100394.

[26] P. van den Driessche, J. Watmough, Reproduction Numbers and Sub-Threshold Endemic Equilibria for Compartmental Models of Disease Transmission, Math. Biosci. 180 (2002), 29–48. https://doi.org/10.1016/s0025-5564(02)00108-6.

[27] J.P. LaSalle, The Stability of Dynamical Systems, SIAM, Philadelphia, 1960.

[28] Z. Shuai, P. van den Driessche, Global Stability of Infectious Disease Models Using Lyapunov Functions, SIAM J. Appl. Math. 73 (2013), 1513–1532. https://doi.org/10.1137/120876642.

[29] O.A. Adepoju, S. Olaniyi, Stability and Optimal Control of a Disease Model With Vertical Transmission and Saturated Incidence, Sci. Afr. 12 (2021), e00800.